Since January 2020 Elsevier has created a COVID-19 resource centre with free information in English and Mandarin on the novel coronavirus COVID-19. The COVID-19 resource centre is hosted on Elsevier Connect, the company's public news and information website.

Science of the Total Environment 745 (2020) 141025

Contents lists available at ScienceDirect

Science of the Total Environment

journal homepage: www.elsevier.com/locate/scitotenv

Influence of Chinese New Year overlapping COVID-19 lockdown on HONO sources in Shijiazhuang

Yongchun Liu [a,*,1], Shuangying Ni [b,1], Tao Jiang [c], Shubin Xing [b], Yusheng Zhang [a], Xiaolei Bao [b,*], Zeming Feng [a], Xiaolong Fan [a], Liang Zhang [d], Haibo Feng [b]

[a] Aerosol and Haze Laboratory, Advanced Innovation Center for Soft Matter Science and Engineering, Beijing University of Chemical Technology, Beijing 100029, China
[b] Hebei Provincial Academy of Environmental Sciences, Shijiazhuang 050037, China
[c] Hebei Provincial Meteorological Technical Equipment Center, Shijiazhuang 050021, China
[d] Hebei Province Environmental Emergency and Heavy Pollution Weather Forewarning Center, 050037, China

HIGHLIGHTS

- High concentration of HONO was observed from 0.08 to 12.67 ppbv in Shijiazhuang.
- Heterogeneous conversion of NO_2 to HONO dominated the nighttime HONO source.
- The lockdown during & after CNY reduced ~31% of ambient HONO.
- Heterogeneous conversion kinetics from NO_2 to HONO increased during & after CNY.
- The *T* and aerosol properties promoted conversion of NO_2 to HONO during & after CNY.

GRAPHICAL ABSTRACT

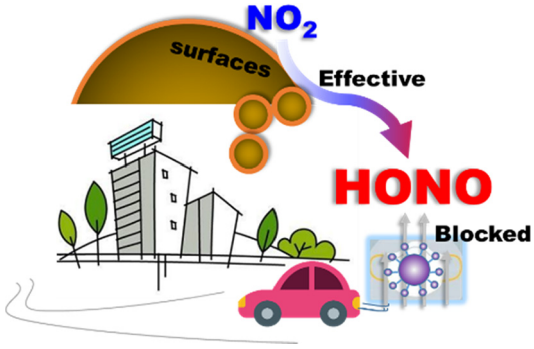

ARTICLE INFO

Article history:
Received 19 June 2020
Received in revised form 13 July 2020
Accepted 15 July 2020
Available online 21 July 2020

Editor: Jianmin Chen

Keywords:
Nitrous acid
Concentrations and sources
Anthropogenic activities
COVID-19
Heterogeneous conversion

ABSTRACT

Nitrous acid (HONO) is an important precursor of hydroxyl radical (OH) in the atmosphere. It is also toxic to human health. In this work, HONO concentrations were measured in Shijiazhuang using a Monitor for AeRosols and Gases in ambient Air (MARGA) from December 15, 2019 to March 15, 2020, which covered the heavy air pollution season, the Chinese New Year (CNY) vocation and the Corona Virus Disease-19 (COVID-19) lockdown period. During & after CNY overlapping COVID-19 lockdown, the air quality was significantly improved because of both the emission reduction and the increase in diffusion ability of air masses. The mean HONO concentration was 2.43 ± 1.08 ppbv before CNY, while it decreased to 1.53 ± 1.16 ppbv during CNY and 0.97 ± 0.76 ppbv after CNY. The lockdown during & after CNY reduced ~31% of ambient HONO along with ~62% of NO and ~36% of NO_2 compared with those before CNY after the improvement of diffusion ability had been taken into consideration. Heterogeneous reaction of NO_2 on ground surface dominated the nocturnal HONO sources, followed by heterogeneous reaction on aerosol surface, vehicle emission, reaction between NO and OH and emission from soil on pollution days throughout the observation. Except for elevated soil emission, other nighttime HONO sources and sinks decreased significantly during & after CNY. The relative importance of heterogeneous reaction of NO_2 on surfaces further increased because of both the decrease in vehicle emission and the increase in the heterogeneous conversion kinetics from NO_2 to HONO during & after CNY.

* Corresponding authors.
E-mail addresses: liuyc@buct.edu.cn (Y. Liu), bxl5@163.com (X. Bao).
[1] These authors contributed equally to this work.

https://doi.org/10.1016/j.scitotenv.2020.141025
0048-9697/

1. Introduction

Nitrous acid (HONO) is a crucial atmospheric species because it is the vital precursor of hydroxyl radical (OH) (Alicke et al., 2003; Ren et al., 2006; Spataro and Ianniello, 2014), which is able to clean up primary air pollutants and produce secondary air pollutants in the atmosphere. Photolysis of H_2O_2, HCHO, O_3 and HONO and the reaction between NO and HO_2 are the major sources of OH radical in the atmosphere (Alicke et al., 2003; Volkamer et al., 2010), whereas photolysis of HONO is the dominant primary OH source in the early morning when other OH sources are still weak (Alicke et al., 2003; Spataro et al., 2013; Tan et al., 2018; Tang et al., 2015; Volkamer et al., 2010). Photolysis of HONO accounts for average up to 60% of OH production in the boundary layer in some cases (Alicke et al., 2003; Elshorbany et al., 2009; Tan et al., 2018). It has been found that HONO is capable of promoting secondary aerosols (Czader et al., 2015; Liu et al., 2020; Xing et al., 2019; Zhang et al., 2019a; Zhang et al., 2019c) and ozone formation (Zhang et al., 2019a). In addition, exposures to high concentration of HONO may damage mucous membranes and result into the respiratory system of asthmatics (Ohyama et al., 2019; Ohyama et al., 2010; Rasmussen et al., 1995). HONO is also a precursor of the mutagenic and carcinogenic nitrosamines via reaction with secondary and tertiary amines (Pitts et al., 1978; Sleiman et al., 2010). Therefore, it is important to investigate the atmospheric HONO from the point view of both atmospheric chemistry and toxicology, in particular, in the regions suffering from heavy air pollution.

Atmospheric HONO has been investigated since the late 1970s (Perner and Platt, 1979). Field experiments were carried out at different environments worldwide in the last few decades (Acker et al., 2006; Crilley et al., 2016; Lee et al., 2016; Levy et al., 2014; Michoud et al., 2014; Spataro and Ianniello, 2014; Zhang et al., 2012a). The HONO concentrations varied from a few pptv in remote areas (Beine et al., 2001; Gu et al., 2020; Honrath et al., 2002; Liao et al., 2006; Spataro et al., 2017; Zhang et al., 2012a; Zhou et al., 2001) to several ppbv in polluted urban environment (Crilley et al., 2016; Hu et al., 2002; Spataro et al., 2013; Zhang et al., 2019e). In China, the concentration and budget of atmospheric HONO have also been extensively studied (Spataro et al., 2013), such as in Beijing (Hendrick et al., 2014; Hu et al., 2002; Spataro et al., 2013; Wang et al., 2017; Zhang et al., 2019e), Shanghai (Wang et al., 2013; Zhang et al., 2019b), Guangzhou (Hu et al., 2002; Su et al., 2008a), Hongkong (Xu et al., 2015), Ji'nan (Li et al., 2018) and Xi'an (Huang et al., 2017). Overall, the HONO concentrations were higher in China than those observed in Europe and America. At the present time, direct emissions from combustion and soil, homogeneous reaction between NO and OH radical, heterogeneous reaction of NO_2 on aerosol and ground surfaces and photolysis reactions of nitrates have been identified as the major sources of atmospheric HONO (Spataro and Ianniello, 2014), whereas their relative contributions depend on the location and the season. For example, heterogeneous reaction of NO_2 was proposed to be an important HONO source in the night (Wang et al., 2017; Zhang et al., 2019c) and even in daytime in Beijing-Tianjin-Hebei (BTH) (Zhang et al., 2019c), but it was unimportant compared with the unknown sources and homogeneous reaction between NO and OH in Ji'nan (Li et al., 2018) or compared with traffic emission on haze days in Beijing (Zhang et al., 2019e). At the same time, the traffic emission was found to be an unimportant HONO source during nighttime in BTH (Zhang et al., 2019c), while it could contribute ~50% to HONO sources on haze days in Beijing (Liu et al., 2020; Meng et al., 2019; Zhang et al., 2019e). In addition, an unknown daytime HONO source, which is highly correlated with light intensity (Lee et al., 2016; Michoud et al., 2014), was frequently observed at various places. More and more studies proposed that it might be associated with photo-enhanced conversion of NO_2 (Michoud et al., 2014; Su et al., 2008b) and photolysis of surface nitrate or particulate nitrates although an uncertainty may reduce their importance (Liu et al., 2019b). These results mean that the study about atmospheric HONO budget is still far from closed, which requires a significant effort on both the HONO measurement and the determination of related kinetic parameters for its production pathways (Liu et al., 2019b).

Shijiazhuang is one of the cities suffering from heavy air pollution in China (Qin et al., 2017; Tan et al., 2019; Xie et al., 2019; Zhang et al., 2020). Fine particulate matter (PM) pollution is more serious in Shijiazhuang than the neighboring areas such as Beijing (Cheng et al., 2019; Qin et al., 2017; Zhang et al., 2019). However, the studies on air pollution regarding both fine particles and HONO are very limited in Shijiazhuang. To the best of our knowledge, there is no publication on the concentration and the source studies of atmospheric HONO in Shijiazhuang. Therefore, it is meaningful to investigate the HONO sources for understanding the complex atmospheric chemistry in Shijiazhuang. In particular, during the Chinese New Year (CNY) in 2020 overlapping the Corona Virus Disease-19 (COVID-19) epidemic, the COVID-19 lockdown led to significant reduction of traffic and industry emissions. This provides us a unique opportunity to understand the influence of anthropogenic activities on atmospheric HONO concentrations and confirm the relative importance among different sources. In this work, we performed continuous field observations of HONO and other air pollutants at an urban station in Shijiazhuang from December 15, 2019 to March 15, 2020. The changes of HONO concentrations and the sources have been discussed during the COVID-19 lockdown compared with that before CNY.

2. Material and methods

2.1. Field measurements

Field measurements were performed at Hebei Atmospheric Supersite, which is located in the campus of Shijiazhuang University (Lat. 38.0281° and Lon. 114.6070°). The observation station (Fig. S1) is on a rooftop of the main teaching building (5 floors, ~23 m above the surface) which is around 250 m from the Zhujiang road. It is a typical urban observation station surrounded by traffic and residential emissions.

Mass concentration of $PM_{2.5}$ was measured by a beta attenuation mass monitor (BAM-1020, Met One Instruments) with a smart heater (Model BX-830, Met One Instruments Inc., USA) to control the RH of the incoming air to 35% and a $PM_{2.5}$ inlet (URG) to cut off the particles with diameter larger than 2.5 μm. Water-soluble ions (Cl^-, NO_3^-, SO_4^{2-}, Na^+, NH_4^+, K^+, Mg^{2+}, and Ca^{2+}) in $PM_{2.5}$ and gas pollutants (HCl, HONO, HNO_3, SO_2 and NH_3) were measured using an analyzer for Monitoring AeRrosols and Gases in ambient Air (MARGA, ADI 2080, Applikon Analytical B.V.) with 1 h of time resolution. Trace gases including NO_x, SO_2, CO and O_3 were measured with the corresponding analyzer (Thermo Scientific, 42i, 43i, 48i and 49i). Meteorological parameters including temperature, pressure, relative humidity (RH), wind speed and direction were measured using a weather station (WXT 520, Vaisala). Planetary boundary layer (PBL) height was measured using a Doppler Lidar (EV-Lidar-CAM, Everise Technology Ltd.). Particles size distribution from 10 to 760 nm was measured with a scanning mobility particle sizer (SMPS, TSI), which is consist of a differential mobility analyzer (DMA 3938, TSI) and a condensation particle counter (CPC 3776, TSI). The particles from 500 to 10,000 nm were measured by an APS (3321, TSI). OC and EC were measured according to the National Institute for Occupational Safety and Health (NIOSH) protocol using an OC/EC analyzer (Model 4, Sunset).

The MARGA was externally calibrated using anionic solutions (Cl^-, Br^-, NO_3^-, SO_4^{2-}) and cationic solutions (Li^+, Na^+, K^+, Mg^{2+} and Ca^{2+}) seasonally. Internal calibration was also hourly carried out using LiBr standard solutions. The detection limit of Cl^-, NO_3^-, SO_4^{2-}, Na^+, NH_4^+, K^+, Mg^{2+}, and Ca^{2+} were 0.01, 0.05, 0.04, 0.05, 0.05, 0.09, 0.06 and 0.09 μg m^{-3}, respectively. All of the instruments for trace gas measurements were calibrated using the corresponding standard gases weekly. The detection limits are 0.05, 0.05, 40, and 0.5 ppbv for NO_x, SO_2, CO and O_3, respectively. External calibration was performed biweekly for the OC/EC analyzer using sucrose solutions.

2.2. HONO budget calculation

The major sources of ambient HONO include direct emission from soil (E_{soil}) (Meusel et al., 2018; Oswald et al., 2015) and vehicle exhaust ($E_{vehicle}$) (Trinh et al., 2017), homogeneous reaction between NO and OH (P_{NO-OH}) in the atmosphere, photolysis of nitrate ($P_{nitrate}$) (Bao et al., 2018), heterogeneous reaction of NO_2 on aerosol surface ($P_{aerosol}$) (Liu et al., 2015) and ground surface (P_{ground}) (Li et al., 2018; Liu et al., 2019b; Wang et al., 2017). Photolysis of HNO_3 and nitrophenol were usually not considered in source budget analysis because they were believed as minor HONO sources (Lee et al., 2016). The sinks of HONO include photolysis ($L_{photolysis}$), the homogeneous reaction with OH radical ($L_{HONO-OH}$), dry deposition ($L_{deposition}$) (Liu et al., 2019b) and vertical and horizontal transport (T_{trans}) (Soergel et al., 2011). Thus, the HONO budget can be calculated by,

$$\frac{dc_{HONO}}{dt} = E_{soil} + E_{vehicle} + P_{NO-OH} + P_{nitrate} + P_{aerosol} + P_{ground} + P_{unknown} - L_{photolysis} - L_{HONO-OH} - L_{deposition} + T_{trans} \quad (1)$$

where $\frac{dc_{HONO}}{dt}$ is the observed change rate of HONO mixing ratios (ppbv h^{-1}), $P_{unknown}$ is the production rate of HONO from the unknown sources.

In our previous work (Liu et al., 2020), the calculation methods for these terms have been discussed in detail. Briefly, the emission rate of HONO (E_{HONO}, ppbv h^{-1}) from soil and vehicle were calculated based on the emission flux (F_{HONO}, g m^{-2} s^{-1}) and the PBL height (H, m) according to the following equation,

$$E_{HONO} = \frac{a \cdot F_{HONO}}{H} \quad (2)$$

where, α is the conversion factor ($\alpha = \frac{1\times10^9\cdot3600\cdot R\cdot T}{M\cdot P} = \frac{2.99\times10^{13}\cdot T}{M\cdot P}$), M is the molecular weight (g mol^{-1}), T is the temperature (K) and P is the atmospheric pressure (Pa). For vehicle emission,

$$F_{HONO,vehicle} = \frac{EI_{HONO},vehice}{A} = \frac{EI_{NOx,vehicle}}{A} \cdot \left(\frac{HONO}{NOx}\right)_{vehicle} \quad (3)$$

where, EI_{HONO} is the emission inventory of HONO (g s^{-1}), A is the urban area of Shijiazhuang (496 km^2, measured based on Google map), $EI_{NOx,vehicle}$ is the emission inventory of NO_x from vehicle exhaust (0.160 Gg day^{-1} in Shijiazhuang before CNY) (Qi et al., 2017). The daily mean $EI_{NOx,vehicle}$ was further converted into hourly mean emission inventory based on the hourly mean traffic index (www.nitrafficindex.com, Fig. S2A) before CNY. During & after CNY, the hourly mean emission inventory of NO_x was further calculated according to its reduction ratio from traffic emission (62% which will be discussed in Section 3.1). The NO_x emission inventories are shown in Fig. S2B and C. The emission ratio of HONO to NO_x (1.26%) was estimated using a low limit correlation method (Li et al., 2012). This value is very close to those derived values in Hongkong (1.2 ± 0.4%, (Xu et al., 2015) and 1.23 ± 0.35% (Liang et al., 2017)), Guangzhou (1.0%) (Li et al., 2012) and Beijing (1.17%, 1.3% and 1.41%) (Liu et al., 2020; Meng et al., 2019; Zhang et al., 2019e). The $F_{HONO,\ soil}$ was calculated using the temperature-dependent emission flux of HONO from grassland with 35–45% of water content (Oswald et al., 2013). Homogeneous reaction between OH and NO was calculated based on the measured NO concentrations and the estimated OH concentrations in the light of second-order reaction. The second-order reaction rate constant (k_{NO-OH}) is 7.2×10^{-12} cm^3 $molecule^{-1}$ s^{-1} (Li et al., 2012). The daytime OH concentration was estimated according to (Li et al., 2018),

$$c_{OH} = \frac{4.1\times10^9\times(J_{O1D})^{0.83}\times(J_{NO_2})^{0.19}\times(140c_{NO_2}+1)}{0.41c_{NO_2}^2+1.7c_{NO_2}+1} \quad (4)$$

where, J_{O1D} and J_{NO2} are the photolysis frequency of O_3 and NO_2 (s^{-1}), respectively, c_{OH} and c_{NO2} are the concentration of OH and NO_2 (molecules cm^{-3}), respectively. The J_{O1D}, J_{NO2} and J_{HONO} (photolysis frequency of HONO) were calculated using the hourly mean solar zenith angle, the longitude and latitude of the observation station under clear sky condition using a box model, then calibrated according to the measured UV light intensity (Liu et al., 2020). The nighttime OH concentration was assumed to be 1.0×10^5 molecules cm^{-3} (Li et al., 2012; Tan et al., 2018). The calculated J values and OH concentrations were shown in Fig. S3. Production rate of HONO from photolysis of nitrate was calculated based the measured nitrate concentrations and the photolysis frequency of nitrate ($J_{nitrate}$). The mean $J_{nitrate}$ value of 8.24×10^{-5} s^{-1} (Bao et al., 2018) was normalized to the measured UV light intensity in this work. Heterogeneous conversion of NO_2 on aerosol and ground surfaces was calculated according to (Huang et al., 2017; Li et al., 2018),

$$k_{het} = \frac{c_{HONO,corr,t_2} - c_{HONO,corr,t_1}}{\overline{c_{NO2}}(t_2 - t_1)} \quad (5)$$

$$c_{HONO,corr} = c_{HONO} - 0.0126c_{NOx} \quad (6)$$

where, k_{het} is the quasi first-order reaction rate constant for heterogeneous conversion from NO_2 to HONO (s^{-1}), $c_{HONO,corr}$ is the corrected HONO concentration after the HONO emitted from vehicle exhaust has been subtracted (ppbv), $\overline{c_{NO2}}$ is the mean NO_2 concentration from t_1 to t_2. The calculated nighttime k_{het} was 0.016 ± 0.006 h^{-1} from December 15, 2019 to March 15, 2020, which is comparable with those derived in urban environment such as Guangzhou (0.016 h^{-1}), Milan (0.012 h^{-1}) and Kathmandu (0.014 h^{-1}), and higher than that in Ji'nan (0.0068 ± 0.0045 h^{-1}) (Li et al., 2018; Xu et al., 2015). Interestingly, the nighttime k_{het} before CNY was 0.012 ± 0.005 h^{-1}, which was significantly lower than that during and after CNY (0.017 ± 0.003 h^{-1}, $P<0.05$). Therefore, the production rates of HONO from heterogeneous reaction in different periods were calculated using the corresponding k_{het}. The contributions of aerosol and ground surfaces to heterogeneous conversion from NO_2 to HONO were further calculated based on the measured surface area to volume ratio of aerosol (S_a, 0.0017 ± 0.0013 m^{-1}) and the estimated ground surface to volume ratio (S_g, 0.0043 ± 0.0018 m^{-1}) according to,

$$S_g = \frac{2.2}{H} \quad (7)$$

where 2.2 is a roughness of urban ground surface (Li et al., 2018). It should be pointed out that direct emission from soil should also be considered in Eq. (6). However, we did not consider it similar to the previous work (Huang et al., 2017; Li et al., 2018) because the ambient concentration of HONO contributed by soil could not be calculated like that from vehicle emission using NO_x as a reference. This might result into some uncertainty for calculating the k_{het} and will be discussed in Section 3.3.

The loss rates of HONO by photolysis ($L_{photolysis}$), homogeneous reaction with OH radicals ($L_{HONO-OH}$) and dry deposition ($L_{deposition}$) (Liu et al., 2019b) were calculated according to the following equations.

$$L_{photolysis} = 3600\cdot J_{HONO}\cdot c_{HONO} \quad (8)$$

$$L_{HONO-OH} = 3600\cdot k_{HONO-OH}\cdot c_{OH}\cdot c_{HONO} \quad (9)$$

$$L_{deposition} = \frac{3600\cdot v_d\cdot c_{HONO}}{H} \quad (10)$$

where, J_{HONO} is the photolysis rate of HONO (s^{-1}), $k_{HONO-OH}$ is the second-order reaction rate constant between HONO and OH (6×10^{-12} cm^3 $molecule^{-1}$ s^{-1}) (Atkinson et al., 2004), and v_d is the dry deposition rate of HONO (0.001 m s^{-1}) (Han et al., 2017). The vertical and horizontal transport was estimate according to Eq. (11),

$$T_{trans} = k_{dilution}\left(c_{HONO} - c_{HONO\,background}\right) \quad (11)$$

where $k_{dilution}$ is a dilution rate (0.23 h^{-1}, including both vertical and horizontal transport) (Dillon et al., 2002), c_{HONO} and $c_{HONO,background}$ is

the HONO concentration at the observation site and background site, respectively (Dillon et al., 2002). In this work, the lowest nighttime HONO concentration was taken as the $c_{HONO,background}$.

3. Results and discussion

3.1. Overview of the air quality during observation

Fig. 1 shows the time series of selected parameters including the concentrations of $PM_{2.5}$, CO, NO_x and HONO (Fig. 1A and B) and the meteorological parameters such as temperature, pressure, wind speed, wind direction and PBL height (Fig. 1C and D) during the observation. The CNY vacation from January 23 to February 2 was highlighted by the light purple column. The temperature increased gradually and the pressure varied from 998 to 1034 hPa during the whole observation (Fig. 1C). Before and during CNY, the frequency of stagnant weather conditions characterized by low wind speed and low PBL height was higher, while the UV light intensity was lower than those after CNY (Fig. 1D). Five light precipitations occurred on December 15, 2019, February 14 and 15, 24 and March 8, 2020. These datasets will be ruled out in following discussion.

Six pollution events before CNY, one during CNY and another six after CNY overlapping the COVID-19 lockdown were identified according to the concentration of $PM_{2.5}$ (Fig. 1A). After strong wind (regardless of wind direction) accompanied with relatively high PBL height cleaning up the air masses (Fig. 1D), a pollution episode gradually built up with a typical duration of 3– 5 days. Interestingly, the $PM_{2.5}$ concentration well kept pace of the reciprocal of the PBL height (Fig. S4A), in particular, before CNY. This means that the sources of $PM_{2.5}$ should be quite stable and the mass loading of fine PM should be greatly determined by the diffusion ability of air masses in Shijiazhuang. As shown in Fig. 1A, the high $PM_{2.5}$ concentration usually coincided with the high RH (> 50%) which is favorable of heterogeneous conversion of gas phase precursors (Hodas et al., 2014; Wang et al., 2016; Wu et al., 2019). In addition, the $PM_{2.5}$ evolved synchronously with CO, especially, before CNY. These results mean that both secondary production and primary emissions contribute to $PM_{2.5}$ accumulation in Shijiazhuang.

Before CNY, the hourly mean $PM_{2.5}$ concentration varied from 7 to 403 μg m^{-3} with a mean value of 137.9 ± 85.8 μg m^{-3} (Fig. 2A). 70.3% of hourly $PM_{2.5}$ concentration was higher than the daily mean air quality standard of China (75 μg m^{-3}) before CNY. This indicates the serious air pollution in Shijiazhuang when compared with other cities, such as Beijing and Tianjin (Fu et al., 2014). During CNY, a pollution event occurred continuously from January 22 to February 1. Although the maximum $PM_{2.5}$ concentration during CNY was lower than that before CNY, the mean $PM_{2.5}$ concentration (173.9 ± 72.7 μg m^{-3}) was higher than that before CNY because of the long-term favorable metrological conditions for pollutants accumulation including high RH (Fig. 1A), low wind speed and low PBL height (Fig. 1D). After CNY, pollution event still happened frequently. However, both the mass concentration of $PM_{2.5}$ and the frequency of pollution event decreased significantly because of both the reduction of primary emission (indicated by CO, Fig. 1A) and the increase in wind speed and PBL height (Fig. 1D). The mean concentration of $PM_{2.5}$ was 76.7 ± 61.4 μg m^{-3}, and 36.1% of hourly mean $PM_{2.5}$ concentration were higher than 75 μg m^{-3} after CNY.

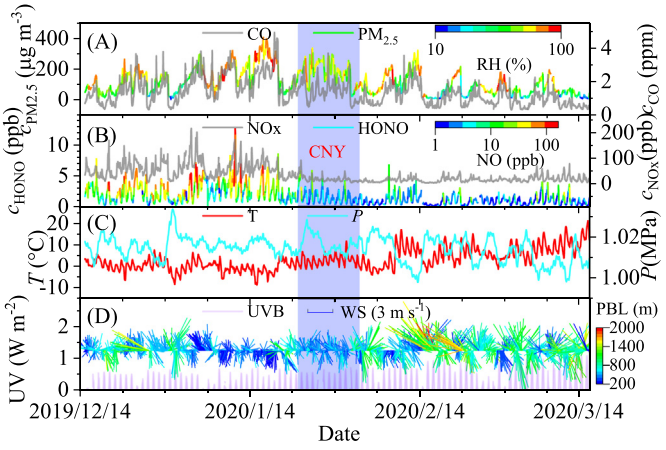

Fig. 1. The time series of (A) $PM_{2.5}$ and CO concentrations, (B) HONO and NO_x concentrations, (C) temperature and pressure and (D) wind direction, wind speed and ultraviolet light intensity from December 15, 2019 to March 15, 2020. The concentrations of $PM_{2.5}$ and HONO are colored by RH and NO concentration, respectively. The wind direction and wind speed are colored by planetary boundary layer (PBL) height. The highlighted period is during Chinese New Year (CNY).

From the point view of chemical composition, the fraction of both nitrate and sulfate increased during and after CNY compared with that before CNY (Fig. S5). The fractions of secondary inorganic aerosol (SIA, including NO_3^-, SO_4^{2-} and NH_4^+) increased significantly from 48.6 ± 13.8% to 53.4 ± 13.6% ($P < 0.05$). The mass ratio of nitrate to sulfate decreased from 1.78 ± 0.78 before CNY to 1.38 ± 0.48 during CNY and then recovered to 1.88 ± 1.08 after CNY (Fig. S4A). This implies that reduction of traffic emission should be prominent during CNY, while both traffic and industry sectors contribute to the emission reduction after CNY overlapping COVID-19 lockdown. In addition, higher conversion ratios of nitrate (NOR) were observed during (0.44 ± 0.11) and after CNY (0.29 ± 0.17) compared with that before CNY (0.17 ± 0.10) (Fig. S6). The above results mean that air quality was greatly improved, while chemical conversion of the precursors to PM was slightly enhanced during and after CNY overlapping COVID-19 lockdown when compared with the counterpart.

The relative change of other pollutants and meteorological parameters including OC, EC, nitrate, SO_2, CO, O_3, NH_3, HONO, NO, NO_2, NO_x, visibility, wind speed, PBL height and CO_2 are shown in Fig. 2. The absolute concentrations of $PM_{2.5}$ components and SO_2 increased significantly during CNY compared with that before CNY, while followed by a decease after CNY. For example, the mean concentration of OC, EC, nitrate and SO_2 were 22.2 ± 7.7, 5.4 ± 2.5, 37.7 ± 17.5 μg m^{-3} and 7.2 ± 2.4 ppbv during CNY, respectively, while the corresponding mean values were 16.1 ± 7.9, 5.1 ± 3.1, 32.7 ± 22.2 μg m^{-3} and 6.4 ± 3.1 ppbv before CNY and 9.8 ± 6.6, 2.3 ± 1.7, 21.5 ± 24.9 μg m^{-3} and 4.5 ± 2.3 ppbv after CNY. The concentration of CO and CO_2 decreased from 1.7 ± 0.9 and 0.49 ± 0.04 ppm before CNY to 1.4 ± 0.6 and 0.47 ± 0.03 during CNY, and further decreased to 1.0 ± 0.5 and 0.45 ± 0.02 ppm after CNY. The concentrations of NO_x well followed $PM_{2.5}$ before CNY, while it slightly increased in the pollution events during and after CNY (Fig. 1). The mean NO_x concentrations were 58.0 ± 33.7, 17.7 ± 12.4 and 15.7 ± 10.4 ppbv before, during and after CNY, respectively. As a more effective tracer of traffic emission, the mean NO concentration decreased from 26.3 ± 26.2 ppbv before CNY to 4.2 ± 6.6 ppbv during CNY and to 3.4 ± 4.4 ppbv after CNY. The concentration of NH_3 was almost constant with the mean concentration of 19.6 ± 10.0, 19.2 ± 5.6, 19.9 ± 11.4 ppbv, respectively, during the three periods. However, the concentration of O_3 increased significantly during CNY (27.5 ± 24.4 ppbv) and after CNY (24.4 ± 13.4 ppbv) compared with that before CNY (7.2 ± 7.9 ppbv) due to increase in UV light (Fig. 1D). The above results indicate that emission reduction from traffic sector is prominent during CNY and after CNY, while industry sector might further contribute to the emission reduction after CNY overlapping the COVID-19 lockdown in Shijiazhuang. To simplify the discussion, the datasets during and after CNY will be combined and marked as during & after CNY in the following section because both periods experienced reduction of anthropogenic activities.

During & after CNY, the reduction ratios of NO, NO_2, NO_x, SO_2, CO, CO_2, $PM_{2.5}$, OC, EC and nitrate were 86.4%, 60.5%, 72.2%, 20.6%, 36.3%, 7.7%, 29.8%, 23.1%, 41.0% and 23.9%, respectively, compared with those before CNY (Fig. 2E). When the background concentrations of CO (235

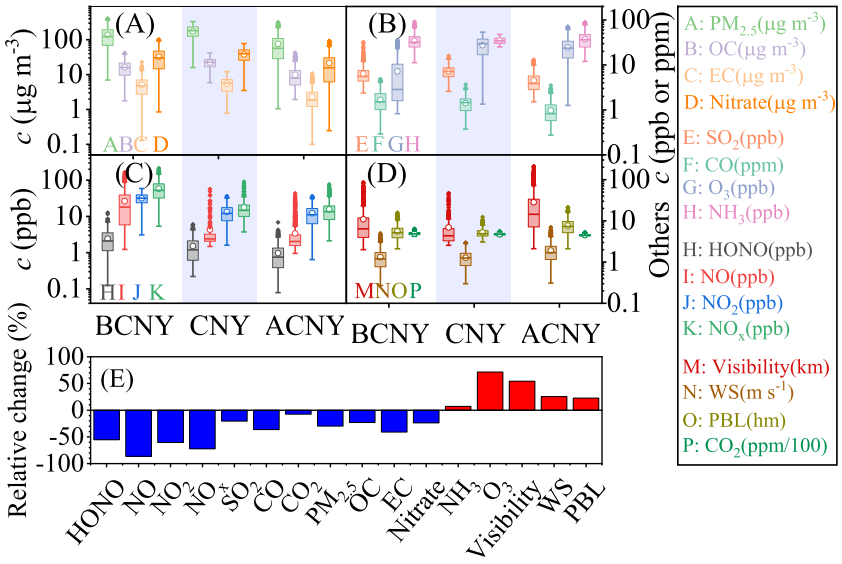

Fig. 2. (A)–(D) Changes of pollutants concentration and meteorological parameters before CNY (BCNY), during CNY and after CNY (ACNY) and (E) relative changes of pollutants and meteorological parameters during & after CNY compared with that before CNY.

ppbv) (Kim et al., 2010) and CO_2 (413 ppm, www.esrl.noaa.gov) were taken into consideration, reduction fraction of CO and CO_2 were 42.2% and 47.1%, respectively. At the same time, the concentration of NH_3 and O_3 increased 7.2% and 71.4%, respectively, during & after CNY compared with before CNY. The visibility increased 54.3% due to the improvement of air quality. The diffusion ability of air masses also increased obviously (~24.1%). For example, the wind speed increased 25.5% and the PBL height increased 22.7% during & after CNY compared with those before CNY. When all of these measured sulfur species (SO_2 and sulfate), nitrogen species (NO, NO_2, HNO_3, HONO and nitrate) and carbon species (CO, CO_2, OC and EC) were taken into consideration, the reduction ratios of total measured sulfur, nitrogen and carbon were 22.7%, 62.8% and 40.8%, respectively, during & after CNY compared with before CNY. This means that ~40% of total nitrogen and ~20% of total carbon reduction might be related to decrease of anthropogenic activities, while reduction of total sulfur might be mainly related to improvement of diffusion ability during & after CNY overlapping COVID-19 lockdown. According to the emission inventory of Hebei province (MEIC v1.3) (Li et al., 2017), transportation sector accounted for 32.6%, 2.6% and 9.1% of NO_x, SO_2 and carbon species emission in 2016, respectively, while the corresponding contribution from industry sector were 51.5%, 72.3% and 61.1%. If we assume that NO measured at our observation site is mainly from traffic emission and the emission profile of NO_x in Shijiazhuang is the same as that in Hebei province, the lockdown during & after CNY overlapping COVID-19 may reduce ~62% (=86.4%-24.1%) of NO_x from traffic emissions and ~ 22% of NO_x from industry emissions after the improvement of diffusion ability has been considered.

3.2. Influence of COVID-19 lockdown on HONO concentration

As shown in Fig. 1B, elevated HONO concentrations were frequently observed during the observation. HONO well followed the $PM_{2.5}$ pollution events before CNY. Increase of HONO concentration was still discernable in each $PM_{2.5}$ pollution event during & after CNY although it was significantly lower than that before CNY. Throughout the observation, the HONO concentration ranged from 0.08 to 12.67 ppbv, with a mean value of 1.64 ± 1.41 ppbv. The maximum hourly value of 12.67 ppbv was recorded in the morning of January 11, 2020. The mean HONO concentration was 2.43 ± 1.08 ppbv before CNY, which was significantly higher than that during CNY (1.53 ± 1.16 ppbv) and after CNY (0.97 ± 0.76 ppbv). 49.7%, 22.4% and 9.1% of hourly mean values exceeding 2.0 ppbv before, during and after CNY, respectively. The nighttime mean HONO concentration was 1.96 ± 1.32 ppbv, compared with that in daytime (1.26 ± 1.43 ppbv) throughout the observation. Before CNY, their corresponding nighttime and daytime mean values were 2.84 ± 1.36 and 1.93 ± 1.76 ppbv, while they were 2.84 ± 1.08 and 1.09 ± 1.10 ppbv during CNY, and 1.19 ± 0.69 and 0.71 ± 0.76 ppbv after CNY.

The mean HONO concentrations before CNY was higher than those reported in foreign cities (Acker et al., 2006; Crilley et al., 2016; Lee et al., 2016; Levy et al., 2014; Michoud et al., 2014; Shon et al., 2007) and several Chinese cities such as Guangzhou(Hu et al., 2002), Hongkong (Xu et al., 2015), Ji'nan (Li et al., 2018) and Xi'an (Huang et al., 2017) as summarized in Table 1, while it was close to these previous observations performed in Beijing (Zhang et al., 2019e) and Shanghai (Cui et al., 2018). Even at noontime (11:00–13:00), the mean HONO concentration was 1.13 ± 1.21 ppbv throughout the observation, and 1.83 ± 1.52, 0.86 ± 0.51, 0.56 ± 0.46 ppbv before, during and after CNY, respectively. Before CNY, 66.7% of the noontime HONO concentrations were higher than 1.00 ppbv, which was the highest level compared with that ever reported in the urban atmospheres. The high HONO concentration observed in this work indicates the intensive HONO sources and potentially strong atmospheric oxidizing capacity in Shijiazhuang. The lockdown during & after CNY overlapping COVID-19 reduced ~55% of HONO concentration, which is ranked the top three pollutants mostly affected by the lockdown along with NO and NO_2 (Fig. 2E). The reduction ratio was ~31% after the improvement of diffusion ability of air masses was subtracted.

Fig. 3 shows the diurnal curves of HONO, NO, NO_2, $PM_{2.5}$, HONO/NO_2 ratio, CO, O_3 and PBL height on clean days ($c_{PM2.5} < 50$ μg m^{-3}) and pollution days ($c_{PM2.5} \geq 50$ μg m^{-3} and RH < 90%). The black and red lines are the diurnal curves before CNY and during & after CNY, respectively. The shadows indicate the standard errors (±1σ). Overall, the nighttime concentrations of HONO, NO, NO_2, HONO/NO_2 ratio and CO were higher than the corresponding daytime values regardless of the pollution level and the period, while O_3 showed an opposite trend due to increase in UV light after sunrise. $PM_{2.5}$ showed relative flat diurnal curves on pollution days although its nighttime concentrations were slightly higher than the daytime concentrations on clean days, in particular, during & after CNY. The PBL height also showed relative flat diurnal curves before CNY, while the slightly elevated PBL heights in daytime were discernable during & after CNY.

The diurnal variation of HONO before CNY was similar to NO, while this similarity disappeared during & after CNY. Their similar nighttime

Table 1
HONO concentrations measured in urban environment.

Observation duration	Location	Instrument	c_{HONO} (ppbv) (median)	References
2001.5–6	Rome, Italy	DOAS	<2	(Acker et al., 2006)
2009.4–5	Houston, USA	ID-CIMS	<1.5(0.19)	(Levy et al., 2014)
2009.7, 2010.1–2	Paris, France	LOPAP	0.01–0.5, 0.01–1.7	(Michoud et al., 2014)
2014.6	York, UK	LOPAP	0.33–1.15	(Crilley et al., 2016)
2014.7–8	London, UK	LOPAP	0.2–1.8	(Lee et al., 2016)
2003.1–2	Kathmandu, Nepal	DOAS	0.15–7.45(1.7)	(Yu et al., 2009)
2004.5–2004.6	Soul, South Korea	WD-IC	1.8 ± 0.4(1.3)	(Shon et al., 2007)
2000.7, 11	Guangzhou, China	GAC	1.0–2.7	(Hu et al., 2002)
2007.8	Beijing, China	WD-IC	1.45 ± 0.58(1.47)	(Spataro et al., 2013)
2011.5, 11	Hongkong, China	LOPAP	0.35 ± 0.30, 0.93 ± 0.67	(Xu et al., 2015)
2014.2–3	Beijing, China	LOPAP	0.28–3.24	(Hou et al., 2016)
2015.7–8	Xi'an, China	LOPAP	1.12 ± 0.97	(Huang et al., 2017)
2006.8–9	Beijing, China	LOPAP, GAC	0.034–3.69	(Yang et al., 2014)
2015.9–10, 2016.1, 4–5, 6–7	Beijing, China	AIM-IC	2.27 ± 1.82; 1.05 ± 89;1.05 ± 0.95; 1.38 ± 0.90	(Wang et al., 2017)
2016.5	Shanghai, China	LOPAP	0.48–5.84(2.31)	(Cui et al., 2018)
2016.12	Beijing, China	LOPAP	3.5 ± 2.7	(Zhang et al., 2019e)
2015.9–2016.8	Jinan, China	LOPAP	1.15 ± 1.07	(Li et al., 2018)
2019.12.15–2020.1.22	Shijiazhuang, China	MARGA	2.43 ± 1.08(2.10)	This work
2019.1.23–2020.2.2			1.53 ± 1.16(1.20)	This work
2019.2.3–2020.2.22			0.97 ± 0.76(0.75)	This work

profiles suggest that vehicle emissions may pose a significant effect on the measured HONO level (Li et al., 2018) before CNY, while other processes such as secondary conversion should become prominent during & after CNY. This was consistent with the fact that high concentration of HONO before CNY was highly correlated with NO concentration (Fig. 1B), while it was well correlated with the HONO/NO_2 ratio during the whole observation (Fig. S4D). The HONO/NO_2 ratio also showed similar diurnal curve of HONO on pollution days, which implies secondary conversion of NO_2 should play an important role in the observed HONO levels. Besides the first peak of HONO/NO_2 in the morning, which is determined by the complex effect among evolution of boundary layer, traffic emission and the photolysis loss of HONO, a second peak of HONO/NO_2 at around noontime (13:00–14:00) during & after CNY was observable on both clean and pollution days. This implies that additional HONO sources may be related to the solar radiation intensity (Lee et al., 2016; Li et al., 2018).

As shown in Fig. 3, diurnal curves of HONO, NO and NO_2 during & after CNY were significantly below those before CNY on both clean days and pollution days. It did so for CO only on pollution days. The diurnal curves of O_3 during & after CNY were significantly above those before CNY. These results further confirmed the reduction of HONO, NO, NO_2 and CO, but the increase of O_3 during & after CNY overlapping COVID-19 lockdown. However, the diurnal variations of $PM_{2.5}$ during & after CNY were only slightly below that before CNY. This might be

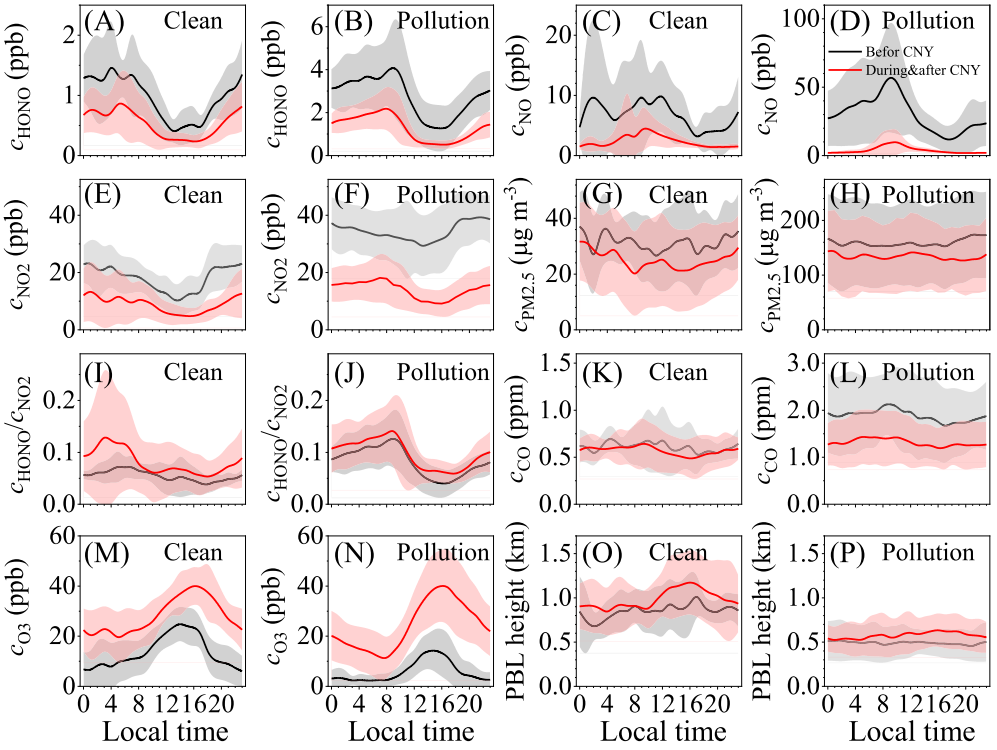

Fig. 3. Diurnal curves of (A) and (B) HONO, (C) and (D) NO, (E) and (F) NO_2, (G) and (H) $PM_{2.5}$, (I) and (J) HONO/NO_2 ratio, (K) and (L) CO, (M) and (N) O_3, (O) and (P) PBL height on clean days ($c_{PM2.5}$ < 50 μg m^{-3}) and pollution days ($c_{PM2.5}$ ≥ 50 μg m^{-3} and RH < 90%). The black lines are the diurnal curves before CNY and the red ones are during & after CNY. The shadows indicate standard errors (±1σ).

related to the weak increase in PBL height during & after CNY compared with that before CNY (Fig. 3O and P). It should be noted that the mean nighttime and daytime HONO/NO_2 ratio were 0.095 ± 0.051 and 0.075 ± 0.053, respectively, throughout the observation. These values are in the range of the reported HONO/NO_2 in literatures (Elshorbany et al., 2009; Huang et al., 2017; Li et al., 2018; Liu et al., 2014; Tong et al., 2015), but at a high level end. Interestingly, the HONO/NO_2 ratio on both clean days and polluted days during & after CNY were slightly higher than the counterpart. This implies that chemical conversion from NO_2 to HONO should be more effective during & after CNY compared with that before CNY. These results also mean that the relative contribution of HONO sources should have changed in different periods.

3.3. Influence of COVID-19 lockdown on HONO sources on pollution days

Fig. 4 compared the budget of HONO before CNY with those during & after CNY on pollution days (with $PM_{2.5}$ concentration > 50 μg m^{-3} and RH <90%). Table S1 summarized the mean intensities of these sources and sinks. Overall, the nighttime sources were comparable with the sinks in different periods, while significant underestimation of the sources presented in the daytime. Besides the possible unknown HONO sources, a possible reason might be related to the variation of PBL height. When we calculating the HONO sources, heterogeneous conversion from NO_2 to HONO and emissions from vehicle and soil were dependent on PBL height according to Eqs. (2) and (7). If these sources were more sensitive to surface HONO concentration (Fig. S4B) than NO_2, the increase in PBL height in daytime should underestimate their contribution to HONO sources. On the other hand, OH concentration was estimated based on J_{O1D} and J_{NO2}. Although the calculated OH concentrations were comparable with that observed in Beijing (Tan et al., 2018), the uncertainty of OH concentration might also contribute the underestimation of HONO sources. In addition, light-enhanced heterogeneous reactions on both aerosol (Liu et al., 2014) and ground surfaces (Liu et al., 2019) have not been considered in this work. This might lead to the observed underestimation. Actually, the contribution of photolysis of nitrate became prominent at noontime, in particular, during & after CNY. This decreased the fraction of the unknown HONO sources. In the following section, we will mainly concentrate on the nighttime HONO sources. However, the unknown sources will also be taken into consideration when we calculating the relative contributions if the total sinks are over the total sources.

In the night, heterogeneous reaction of NO_2 on ground surface was the largest HONO source, followed by heterogeneous reaction on aerosol surface, vehicle emission, homogeneous reaction between NO and OH and soil emission in the whole observation period (Fig. 4). Emission from soil was a minor HONO source during our observation due to the low temperature. E_{soil} varied from 0.00044 to 0.0091 ppbv h^{-1}, with a mean value of 0.0026 ± 0.0014 ppbv h^{-1} throughout the observation. It was slightly higher during & after CNY (0.0031 ± 0.0016 ppbv h^{-1}) than that before CNY (0.0020 ± 0.0008 ppbv h^{-1}) because of the increase in temperature (Fig. 1C). The nighttime E_{soil} were 0.0020 ± 0.0007 ppbv h^{-1} before CNY and 0.0030 ± 0.0015 ppbv h^{-1} during & after CNY, respectively. The corresponding relative contributions to nighttime HONO sources were (0.27 ± 0.08) % and (0.83 ± 0.36) %. Direct emission from vehicle exhaust was an important HONO source. $E_{vehicle}$ ranged from 0.015 to 0.45 ppbv h^{-1}, with a mean value of 0.099 ± 0.078 ppbv h^{-1} throughout the observation. It decreased from 0.16 ± 0.081 ppbv h^{-1} before CNY to 0.052 ± 0.022 ppbv h^{-1} during & after CNY due to the reduction of vehicle emission. The corresponding nighttime values were 0.16 ± 0.078 and 0.051 ± 0.021 ppbv h^{-1}, which contributed 22.2 ± 6.7% (BCNY) and 14.7 ± 5.9% (CNY&ACNY) to HONO sources. These relative contributions were close to that in Ji'nan (12%–21%) (Li et al., 2018), while they were much lower than that in Beijing (~50%) (Liu et al., 2020; Meng et al., 2019; Zhang et al., 2019e). This can be well explained by the fact that the vehicle population in Shijiazhuang is much smaller than that in Beijing (http://www.stats.gov.cn). Because the NO concentrations were very high before CNY (Fig. 1), homogeneous reaction between NO and OH played an important role in HONO source in the night. The nighttime $P_{NO\text{-}OH}$ was 0.076 ± 0.091 ppbv h^{-1} before CNY, while it decreased to 0.0092 ± 0.014 ppbv h^{-1} during & after CNY. Their corresponding fractions in the nighttime HONO sources were 10.8 ± 6.0% and 2.2 ± 1.1%. Compared with above sources, heterogeneous conversion of NO_2 on aerosol and ground surfaces were the most important nighttime HONO source in Shijiazhuang. This is consistent with the high HONO/NO_2 as shown in Fig. 3. The nighttime $P_{aerosol}$ were 0.14 ± 0.08 ppbv h^{-1} before CNY, which was only second to the P_{ground} (0.30 ± 0.12 ppbv h^{-1}). During & after CNY, they were 0.069 ± 0.055 ppbv h^{-1} ($P_{aerosol}$) and 0.20 ± 0.12 ppbv h^{-1} (P_{ground}), respectively. Thus, heterogeneous reaction of NO_2 on aerosol surface contributed 19.0 ± 3.9% to the nighttime HONO sources before CNY. It increased to 21.2 ± 5.7% during & after CNY due to the decrease of $E_{vehicle}$ and $P_{NO\text{-}OH}$. The relative contribution of ground surface increased from 38.9 ± 7.8% before CNY to 48.0 ± 13.1% during & after CNY. Photolysis was the major loss of HONO in the daytime. Before CNY, it was 2.65 ± 2.77 ppbv h^{-1}, while it decreased to 1.59 ± 1.86 ppbv h^{-1} during & after CNY. In the night,

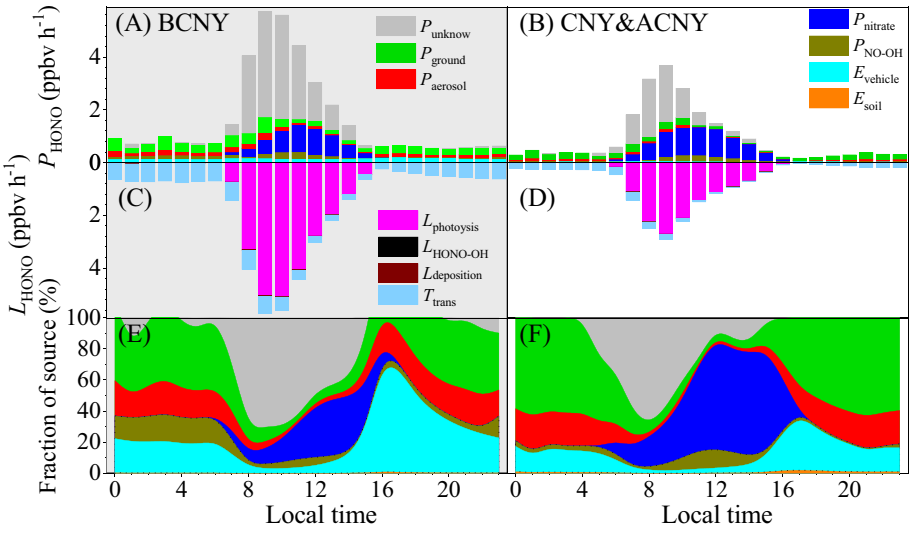

Fig. 4. HONO budget before CNY and during & after CNY on polluted days with $PM_{2.5}$ concentration > 50 μg m^{-3} and RH <90%.

vertical and horizontal transport dominated the sinks of HONO, with a mean value of 0.60 ± 0.31 ppbv h^{-1} before CNY and 0.26 ± 0.19 ppbv h^{-1} during & after CNY.

Except for E_{soil} (increased 50%), the reduction ratio of all other sources and sinks ranged from 33% to 88% in the night during & after CNY when compared with that before CNY as shown in Table S1. In the daytime, besides E_{soil}, $P_{nitrate}$ and $L_{HONO\text{-}OH}$ increased 18% and 67%, respectively, whereas other sources and sinks decreased from 40% to 68%. The increase of E_{soil} was related to increase in temperature, while it was related to increase in irradiation intensity for $P_{nitrate}$ and increase in OH concentrations for $L_{HONO\text{-}OH}$. In the night, vehicle related sources ($E_{vehicle}$ and $P_{NO\text{-}OH}$) were the mostly influenced sources, while heterogeneous conversion (in particular, on ground surface) was less affected by the reduction of anthropogenic activities during and after CNY overlapping COVID-19. Therefore, this led to an increased relative contribution of heterogeneous reaction on ground and aerosol surfaces in the night (Fig. 4). This is consistent with the good correlation between HONO concentrations and NO, NO_2 and $PM_{2.5}$ concentrations as shown in Fig. S7.

As pointed above, the k_{het} during & after CNY (0.017 ± 0.003 h^{-1}, $P < 0.05$) was significantly higher than that before CNY (0.012 ± 0.005 h^{-1}). We further derived the uptake coefficient of NO_2 (γ_{NO2}) on both aerosol and ground surfaces according to,

$$k_{het} = \frac{S\omega\gamma_{NO_2}}{4} \quad (12)$$

$$\omega = \sqrt{\frac{8RT}{\pi M}} \quad (13)$$

where, S is the total surface to volume ratio of ground and aerosols ($S_g + S_a$, m^{-1}), ω is the mean velocity of NO_2 molecules, R is the ideal gas constant, T is the temperature (K), M is the molecular weight of NO_2 (kg mol^{-1}). Fig. 5A compared the derived nighttime γ_{NO2} before CNY with that during & after CNY. It was 6.43 ± 9.02 × 10^{-6} before CNY, which is significantly ($P < 0.05$) lower than 1.20 ± 1.76 × 10^{-5} during & after CNY. These values are larger than that derived in Ji'nan (1.4 ± 2.4 × 10^{-6}) (Li et al., 2018) and the laboratory values (5 × 10^{-9} - 9.6 × 10^{-6}) on different particles (Ndour et al., 2009; Underwood et al., 1999; Underwood et al., 2001). The elevated γ_{NO2} means that reaction kinetic is favorable of heterogeneous conversion from NO_2 to HONO during & after CNY although both NO_2 and $PM_{2.5}$ concentrations decreased compared with before CNY. As pointed in Section 2.2, direct emission of HONO from soil was not considered when we calculating the k_{het}. This will lead to an additional uncertainty for the γ_{NO2}. However, this uncertainty should be small because the emission rate of HONO from vehicle (0.099 ± 0.078 ppbv h^{-1}) was as ~38 times as that from soil (0.0026 ± 0.0014 ppbv h^{-1}).

As shown in Fig. 5B, the γ_{NO2} is well negatively correlated with the reciprocal of temperature ($\ln\gamma_{NO2} = -2.46 \times 10^3/T$-2.69, $R = 0.92$). This means the conversion from NO_2 to HONO requires to overcome an apparent activation energy (20.5 kJ mol^{-1}). Thus, the higher nighttime temperature (278.0 ± 4.1 K) during & after CNY was favorable of this reaction compared with that before CNY (272.7 ± 2.6 K). On the other hand, the γ_{NO2} was negatively correlated with both the ratio of aerosol water content to $PM_{2.5}$ mass concentration ($AWC/PM_{2.5}$) and the aerosol acidity (pH), which were calculated using the ISORROPIA-II model with the gas phase and particle phase concentrations of the relevant species, the temperature and the RH as inputs in a forward mode under metastable conditions (Ding et al., 2019). The corresponding equation is $\gamma_{NO2} = 1.28 \times 10^{-5}$-$6.71 \times 10^{-6}$ $AWC/PM_{2.5}$ ($R = 0.71$) and $\gamma_{NO2} = 1.79 \times 10^{-5}$-$1.24 \times 10^{-6}$ pH ($R = 0.57$) (Fig. 5C and D). Both the nocturnal $AWC/PM_{2.5}$ ratio (0.31 ± 0.27) and aerosol pH (4.87 ± 0.89) during & after CNY were significantly lower than those values (0.35 ± 0.31 and 5.17 ± 1.19) before CNY. This can be explained by the higher SIA fraction (Fig. S3) and the lower RH during & after CNY. These results are well agreement with previous laboratory studies that water can competitively inhibit the uptake of NO_2 (Liu et al., 2015; Zhang et al., 2012b) and particle phase acids can promote HONO formation from heterogeneous reaction of NO_2 (Bao et al., 2018; Han et al., 2016). This means the variation of aerosol properties might be another reason lead to the elevated reactivity for heterogeneous conversion from NO_2 to HONO during & after CNY. Thus, the increase in the relative contribution of heterogeneous reactions on ground and aerosol surfaces can be explained by both the

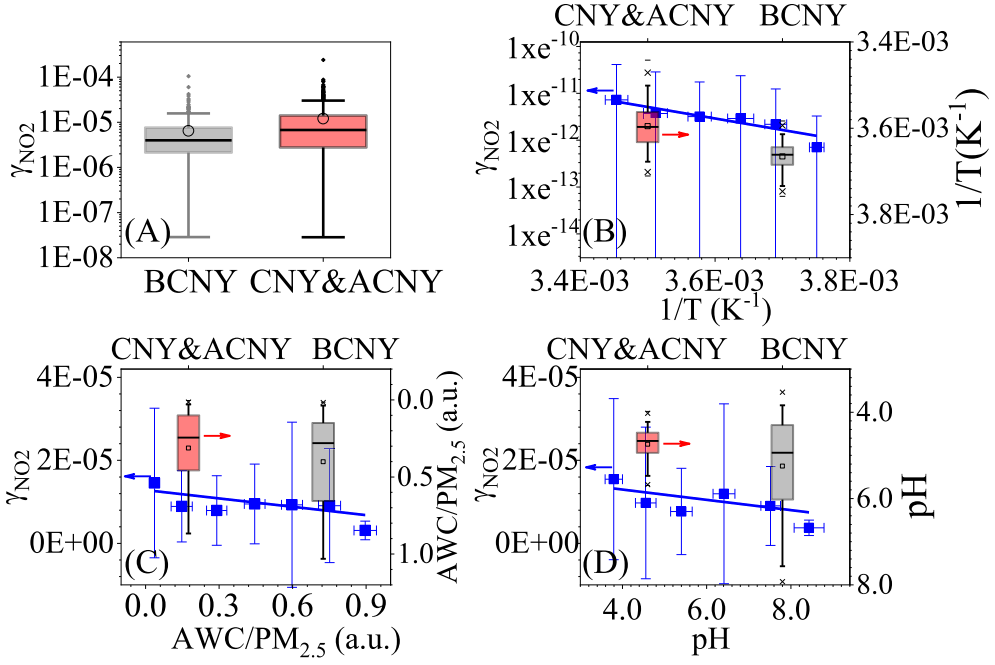

Fig. 5. (A) The derived nighttime γ_{NO2} before CNY and during & after CNY, the dependence of the γ_{NO2} on (B) the temperature, (c) the ratio of $AWC/PM_{2.5}$ and the aerosol pH. The box plots in (B)–(D) are the distribution of nighttime temperature, $AWC/PM_{2.5}$ and aerosol pH before CNAY and during & after CNY.

effective heterogeneous conversion from NO_2 to HONO and the reduction of direct emission from vehicle.

4. Conclusions

During & after CNY overlapping COVID-19 lockdown, great reduction of air pollutants emission was observed in Shijiazhuang. The reduction ratio of NO, NO_2, NO_x, SO_2, CO, CO_2, $PM_{2.5}$, OC, EC and nitrate concentrations were 86.4%, 60.5%, 72.2%, 20.6%, 42.2%, 47.1%, 29.8%, 23.1%, 41.0% and 23.9%, respectively, compared with those before CNY. At the same time, the diffusion ability of air mass increased obviously as evident by the increase in wind speed (25.5%) and PBL height (22.7%) during & after CNY. The lockdown during & after CNY overlapping COVID-19 might reduce ~62% of NO_x from traffic emissions after improvement of diffusion ability was taken into consideration.

The mean HONO concentration was 2.43 ± 1.08 ppbv before CNY, which was significantly higher than those during CNY (1.53 ± 1.16 ppbv) and after CNY (0.97 ± 0.76 ppbv). The lockdown during & after CNY overlapping COVID-19 reduced ~31% of ambient HONO compared with that before CNY after the improvement of diffusion ability was considered. Heterogeneous reaction of NO_2 on ground surface was the largest nocturnal HONO source, followed by heterogeneous reaction on aerosol surface, vehicle emission, homogeneous reaction between NO and OH and emission from soil in the observation period. Except for emission from soil, most of the HONO sources and sinks decreased from 33% to 88% in the night during & after CNY when compared with that before CNY. The relative importance of heterogeneous reaction of NO_2 on surfaces further increased during & after CNY because of both the decrease in vehicle emission and the increase in heterogeneous reaction kinetics compared with that before CNY. This work confirmed that reducing anthropogenic activities definitely reduced ambient HONO concentrations, while it nonlinearly responded to the reduction of anthropogenic activities.

CRediT authorship contribution statement

Yongchun Liu: Conceptualization, Methodology, Data curation, Writing - original draft. **Shuangying Ni:** Conceptualization, Methodology, Investigation, Writing - original draft. **Tao Jiang:** Investigation, Resources. **Shubin Xing:** Investigation, Resources, Writing - review & editing. **Yusheng Zhang:** Investigation, Data curation. **Xiaolei Bao:** Conceptualization, Methodology, Data curation, Investigation, Resources, Writing - original draft. **Zeming Feng:** Investigation, Data curation. **Xiaolong Fan:** Investigation, Data curation. **Liang Zhang:** Investigation, Data curation. **Haibo Feng:** Writing - review & editing, Funding acquisition.

Declaration of competing interest

The authors declare that they have no conflict of interest.

Acknowledgements

This research was financially supported by the Ministry of Science and Technology of the People's Republic of China (2019YFC0214701), the National Natural Science Foundation of China (41877306), the Strategic Priority Research Program of Chinese Academy of Sciences and Beijing University of Chemical Technology.

Appendix A. Supplementary data

Supplementary data to this article can be found online at https://doi.org/10.1016/j.scitotenv.2020.141025.

References

Acker, K., Febo, A., Trick, S., Perrino, C., Bruno, P., Wiesen, P., Möller, D., Wieprecht, W., Auel, R., Giusto, M., Geyer, A., Platt, U., Allegrini, I., 2006. Nitrous acid in the urban area of Rome. Atmos. Environ. 40, 3123–3133.

Alicke, B., Geyer, A., Hofzumahaus, A., Holland, F., Konrad, S., Patz, H.W., Schafer, J., Stutz, J., Volz-Thomas, A., Platt, U., 2003. OH formation by HONO photolysis during the BERLIOZ experiment. J. Geophys. Res.-Atmos. 108, 17.

Atkinson, R., Baulch, D.L., Cox, R.A., Crowley, J.N., Hampson, R.F., Hynes, R.G., Jenkin, M.E., Rossi, M.J., Troe, J., 2004. Evaluated kinetic and photochemical data for atmospheric chemistry: volume I - gas phase reactions of Ox, HOx, NOx and SOx species. Atmos. Chem. Phys. 4, 1461–1738.

Bao, F., Li, M., Zhang, Y., Chen, C., Zhao, J., 2018. Photochemical aging of Beijing urban $PM_{2.5}$: HONO production. Environ. Sci. Technol. 52, 6309–6316.

Beine, H.J., Allegrini, I., Sparapani, R., Ianniello, A., Valentini, F., 2001. Three years of spring-time trace gas and particle measurements at Ny-Ålesund, Svalbard. Atmos. Environ. 35, 3645–3658.

Cheng, J., Su, J., Cui, T., Li, X., Dong, X., Sun, F., Yang, Y., Tong, D., Zheng, Y., Li, Y., Li, J., Zhang, Q., He, K., 2019. Dominant role of emission reduction in $PM_{2.5}$ air quality improvement in Beijing during 2013–2017: a model-based decomposition analysis. Atmos. Chem. Phys. 19, 6125–6146.

Crilley, L.R., Kramer, L., Pope, F.D., Whalley, L.K., Cryer, D.R., Heard, D.E., Lee, J.D., Reed, C., Bloss, W.J., 2016. On the interpretation of in situ HONO observations via photochemical steady state. Faraday Discuss. 189, 191–212.

Cui, L., Li, R., Zhang, Y., Meng, Y., Fu, H., Chen, J., 2018. An observational study of nitrous acid (HONO) in Shanghai, China: the aerosol impact on HONO formation during the haze episodes. Sci. Total Environ. 630, 1057–1070.

Czader, B.H., Choi, Y., Li, X., Alvarez, S., Lefer, B., 2015. Impact of updated traffic emissions on HONO mixing ratios simulated for urban site in Houston, Texas. Atmos. Chem. Phys. 15, 1253–1263.

Dillon, M.B., Lamanna, M.S., Schade, G.W., Goldstein, A.H., Cohen, R.C., 2002. Chemical evolution of the Sacramento urban plume: transport and oxidation. J. Geophys. Res. Atmos. 107, ACH 3–1-ACH 3-15.

Ding, J., Zhao, P., Su, J., Dong, Q., Du, X., Zhang, Y., 2019. Aerosol pH and its driving factors in Beijing. Atmos. Chem. Phys. 19, 7939–7954.

Elshorbany, Y.F., Kurtenbach, R., Wiesen, P., Lissi, E., Rubio, M., Villena, G., Gramsch, E., Rickard, A.R., Pilling, M.J., Kleffmann, J., 2009. Oxidation capacity of the city air of Santiago, Chile. Atmos. Chem. Phys. 9, 2257–2273.

Fu, G.Q., Xu, W.Y., Yang, R.F., Li, J.B., Zhao, C.S., 2014. The distribution and trends of fog and haze in the North China Plain over the past 30 years. Atmos. Chem. Phys. 14, 11949–11958.

Gu, R.R., Zheng, P.G., Chen, T.S., Dong, C., Wang, Y.N., Liu, Y.M., Liu, Y.H., Luo, Y.Y., Han, G.X., Wang, X.F., Zhou, X.H., Wang, T., Wang, W.X., Xue, L.K., 2020. Atmospheric nitrous acid (HONO) at a rural coastal site in North China: seasonal variations and effects of biomass burning. Atmos. Environ. 229, 11.

Han, C., Yang, W., Wu, Q., Yang, H., Xue, X., 2016. Key role of pH in the photochemical conversion of NO_2 to HONO on humic acid. Atmos. Environ. 142, 296–302.

Han, X., Zhang, M.G., Skorokhod, A., Kou, X.X., 2017. Modeling dry deposition of reactive nitrogen in China with RAMS-CMAQ. Atmos. Environ. 166, 47–61.

Hendrick, F., Muller, J.F., Clemer, K., Wang, P., De Maziere, M., Fayt, C., Gielen, C., Hermans, C., Ma, J.Z., Pinardi, G., Stavrakou, T., Vlemmix, T., Van Roozendael, M., 2014. Four years of ground-based MAX-DOAS observations of HONO and NO_2 in the Beijing area. Atmos. Chem. Phys. 14, 765–781.

Hodas, N., Sullivan, A.P., Skog, K., Keutsch, F.N., Collett, J.L., Decesari, S., Facchini, M.C., Carlton, A.G., Laaksonen, A., Turpin, B.J., 2014. Aerosol liquid water driven by anthropogenic nitrate: implications for lifetimes of water-soluble organic gases and potential for secondary organic aerosol formation. Environ Sci Technol 48, 11127–11136.

Honrath, R.E., Lu, Y., Peterson, M.C., Dibb, J.E., Arsenault, M.A., Cullen, N.J., Steffen, K., 2002. Vertical fluxes of NOx, HONO, and HNO_3 above the snowpack at Summit, Greenland. Atmos. Environ. 36, 2629–2640.

Hou, S., Tong, S., Ge, M., An, J., 2016. Comparison of atmospheric nitrous acid during severe haze and clean periods in Beijing, China. Atmos. Environ. 124, 199–206.

Hu, M., Zhou, F., Shao, K., Zhang, Y., Tang, X., Slanina, J., 2002. Diurnal variations of aerosol chemical compositions and related gaseous pollutants in Beijing and Guangzhou. J Environ Sci Health, Part A 37, 479–488.

Huang, R.-J., Yang, L., Cao, J., Wang, Q., Tie, X., Ho, K.-F., Shen, Z., Zhang, R., Li, G., Zhu, C., Zhang, N., Dai, W., Zhou, J., Liu, S., Chen, Y., Chen, J., O'Dowd, C.D., 2017. Concentration and sources of atmospheric nitrous acid (HONO) at an urban site in Western China. Sci. Total Environ. 593, 165–172.

Kim, H.S., Chung, Y.S., Tans, P.P., 2010. On the regional distributions of background carbon monoxide concentrations observed in East Asia during 1991–2008. Asia-Pacific J Atmos Sci 46, 89–95.

Lee, J.D., Whalley, L.K., Heard, D.E., Stone, D., Dunmore, R.E., Hamilton, J.F., Young, D.E., Allan, J.D., Laufs, S., Kleffmann, J., 2016. Detailed budget analysis of HONO in central London reveals a missing daytime source. Atmos. Chem. Phys. 16, 2747–2764.

Levy, M., Zhang, R., Zheng, J., Zhang, A.L., Xu, W., Gomez-Hernandez, M., Wang, Y., Olaguer, E., 2014. Measurements of nitrous acid (HONO) using ion drift-chemical ionization mass spectrometry during the 2009 SHARP field campaign. Atmos. Environ. 94, 231–240.

Li, X., Brauers, T., Häseler, R., Bohn, B., Fuchs, H., Hofzumahaus, A., Holland, F., Lou, S., Lu, K.D., Rohrer, F., Hu, M., Zeng, L.M., Zhang, Y.H., Garland, R.M., Su, H., Nowak, A., Wiedensohler, A., Takegawa, N., Shao, M., Wahner, A., 2012. Exploring the atmospheric chemistry of nitrous acid (HONO) at a rural site in Southern China. Atmos. Chem. Phys. 12, 1497–1513.

Li, M., Zhang, Q., Kurokawa, J.I., Woo, J.H., He, K., Lu, Z., Ohara, T., Song, Y., Streets, D.G., Carmichael, G.R., Cheng, Y., Hong, C., Huo, H., Jiang, X., Kang, S., Liu, F., Su, H., Zheng,

B., 2017. MIX: a mosaic Asian anthropogenic emission inventory under the international collaboration framework of the MICS-Asia and HTAP. Atmos. Chem. Phys. 17, 935–963.
Li, D., Xue, L., Wen, L., Wang, X., Chen, T., Mellouki, A., Chen, J., Wang, W., 2018. Characteristics and sources of nitrous acid in an urban atmosphere of northern China: results from 1-yr continuous observations. Atmos. Environ. 182, 296–306.
Liang, Y., Zha, Q., Wang, W., Cui, L., Lui, K.H., Ho, K.F., Wang, Z., Lee, S.-c., Wang, T., 2017. Revisiting nitrous acid (HONO) emission from on-road vehicles: a tunnel study with a mixed fleet. J. Air Waste Manage. Assoc. 67, 797–805.
Liao, W., Case, A.T., Mastromarino, J., Tan, D., Dibb, J.E., 2006. Observations of HONO by laser-induced fluorescence at the South Pole during ANTCI 2003. Geophys. Res. Lett. 33.
Liu, Z., Wang, Y., Costabile, F., Amoroso, A., Zhao, C., Huey, L.G., Stickel, R., Liao, J., Zhu, T., 2014. Evidence of aerosols as a media for rapid daytime HONO production over China. Environ Sci Technol 48, 14386–14391.
Liu, Y., Han, C., Ma, J., Bao, X., He, H., 2015. Influence of relative humidity on heterogeneous kinetics of NO_2 on kaolin and hematite. Phys. Chem. Chem. Phys. 17, 19424–19431.
Liu, J., Li, S., Mekic, M., Jiang, H., Zhou, W., Loisel, G., Song, W., Wang, X., Gligorovski, S., 2019. Photoenhanced uptake of NO_2 and HONO formation on real urban grime. Environ. Sci. Technol. Lett. 6, 413–417.
Liu, Y.H., Lu, K.D., Li, X., Dong, H.B., Tan, Z.F., Wang, H.C., Zou, Q., Wu, Y.S., Zeng, L.M., Hu, M., Min, K.E., Kecorius, S., Wiedensohler, A., Zhang, Y.H., 2019b. A comprehensive model test of the HONO sources constrained to field measurements at Rural North China Plain. Environ Sci Technol 53, 3517–3525.
Liu, Y., Zhang, Y., Lian, C., Yan, C., Feng, Z., Zheng, F., Fan, X., Chen, Y., Wang, W., Chu, B., Wang, Y., Cai, J., Du, W., Daellenbach, K.R., Kangasluoma, J., Bianchi, F., Kujansuu, J., Petäjä, T., Wang, X., Hu, B., Wang, Y., Ge, M., He, H., Kulmala, M., 2020. The promotion effect of nitrous acid on aerosol formation in wintertime Beijing: possible contribution of traffic-related emission. Atmos Chem Phys Discuss 2020, 1–43.
Meng, F., Qin, M., Tang, K., Duan, J., Fang, W., Liang, S., Ye, K., Xie, P., Sun, Y., Xie, C., Ye, C., Fu, P., Liu, J., Liu, W., 2019. High resolution vertical distribution and sources of HONO and NO_2 in the nocturnal boundary layer in urban Beijing, China. Atmos. Chem. Phys. Discuss. 2019, 1–34.
Meusel, H., Tamm, A., Kuhn, U., Wu, D., Leifke, A.L., Fiedler, S., Ruckteschler, N., Yordanova, P., Lang-Yona, N., Poehlker, M., Lelieveld, J., Hoffmann, T., Poeschl, U., Su, H., Weber, B., Cheng, Y., 2018. Emission of nitrous acid from soil and biological soil crusts represents an important source of HONO in the remote atmosphere in Cyprus. Atmos. Chem. Phys. 18, 799–813.
Michoud, V., Colomb, A., Borbon, A., Miet, K., Beekmann, M., Camredon, M., Aumont, B., Perrier, S., Zapf, P., Siour, G., Ait-Helal, W., Afif, C., Kukui, A., Furger, M., Dupont, J.C., Haeffelin, M., Doussin, J.F., 2014. Study of the unknown HONO daytime source at a European suburban site during the MEGAPOLI summer and winter field campaigns. Atmos. Chem. Phys. 14, 2805–2822.
Ndour, M., Nicolas, M., D'Anna, B., Ka, O., George, C., 2009. Photoreactivity of NO2 on mineral dusts originating from different locations of the Sahara desert. Phys. Chem. Chem. Phys. 11, 1312–1319.
Ohyama, M., Oka, K., Adachi, S., Takenaka, N., 2010. Effects of nitrous acid exposure on pulmonary tissues in guinea pigs. Inhal. Toxicol. 22, 930–936.
Ohyama, M., Nakajima, T., Minejima, C., Azuma, K., Oka, K., Itano, Y., Kudo, S., Takenaka, N., 2019. Association between indoor nitrous acid, outdoor nitrogen dioxide, and asthma attacks: results of a pilot study. Int. J. Environ. Health Res. 29, 632–642.
Oswald, R., Behrendt, T., Ermel, M., Wu, D., Su, H., Cheng, Y., Breuninger, C., Moravek, A., Mougin, E., Delon, C., Loubet, B., Pommerening-Röser, A., Sörgel, M., Pöschl, U., Hoffmann, T., Andreae, M.O., Meixner, F.X., Trebs, I., 2013. HONO emissions from soil Bacteria as a major source of atmospheric reactive nitrogen. Science 341, 1233–1235.
Oswald, R., Ermel, M., Hens, K., Novelli, A., Ouwersloot, H.G., Paasonen, P., Petäjä, T., Sipilä, M., Keronen, P., Bäck, J., Königstedt, R., Hosaynali Beygi, Z., Fischer, H., Bohn, B., Kubistin, D., Harder, H., Martinez, M., Williams, J., Hoffmann, T., Trebs, I., Sörgel, M., 2015. A comparison of HONO budgets for two measurement heights at a field station within the boreal forest in Finland. Atmos. Chem. Phys. 15, 799–813.
Perner, D., Platt, U., 1979. Detection of nitrous acid in the atmosphere by differential optical absorption. Geophys. Res. Lett. 6, 917–920.
Pitts, J.N., Grosjean, D., Van Cauwenberghe, K., Schmid, J.P., Fitz, D.R., 1978. Photooxidation of aliphatic amines under simulated atmospheric conditions: formation of nitrosamines, nitramines, amides, and photochemical oxidant. Environ Sci Technol 12, 946–953.
Qi, J., Zheng, B., Li, M., Yu, F., Chen, C.C., Liu, F., Zhou, X.F., Yuan, J., Zhang, Q., He, K.B., 2017. A high-resolution air pollutants emission inventory in 2013 for the Beijing-Tianjin-Hebei region, China. Atmos. Environ. 170, 156–168.
Qin, K., Wang, L.Y., Wu, L.X., Xu, J., Rao, L.L., Letu, H., Shi, T.W., Wang, R.F., 2017. A campaign for investigating aerosol optical properties during winter hazes over Shijiazhuang, China. Atmos. Res. 198, 113–122.
Rasmussen, T.R., Brauer, M., Kjaergaard, S., 1995. Effects of nitrous acid exposure on human mucous membranes. Am. J. Respir. Crit. Care Med. 151, 1504–1511.
Ren, X., Brune, W.H., Mao, J., Mitchell, M.J., Lesher, R.L., Simpas, J.B., Metcalf, A.R., Schwab, J.J., Cai, C., Li, Y., Demerjian, K.L., Felton, H.D., Boynton, G., Adams, A., Perry, J., He, Y., Zhou, X., Hou, J., 2006. Behavior of OH and HO_2 in the winter atmosphere in New York City. Atmos. Environ. 40, 252–263.
Shon, Z.H., Lee, G., Song, S.K., Lee, M., Han, J., Lee, D., 2007. Characteristics of reactive nitrogen compounds and other relevant trace gases in the atmosphere at urban and rural areas of Korea during May–June, 2004. J. Atmos. Chem. 58, 203–218.
Sleiman, M., Gundel, L.A., Pankow, J.F., Jacob 3rd, P., Singer, B.C., Destaillats, H., 2010. Formation of carcinogens indoors by surface-mediated reactions of nicotine with nitrous acid, leading to potential thirdhand smoke hazards. Proc. Natl. Acad. Sci. U. S. A. 107, 6576–6581.
Soergel, M., Regelin, E., Bozem, H., Diesch, J.M., Drewnick, F., Fischer, H., Harder, H., Held, A., Hosaynali-Beygi, Z., Martinez, M., Zetzsch, C., 2011. Quantification of the unknown HONO daytime source and its relation to NO_2. Atmos. Chem. Phys. 11, 10433–10447.
Spataro, F., Ianniello, A., 2014. Sources of atmospheric nitrous acid: state of the science, current research needs, and future prospects. J. Air Waste Manage. Assoc. 64, 1232–1250.
Spataro, F., Ianniello, A., Esposito, G., Allegrini, I., Zhu, T., Hu, M., 2013. Occurrence of atmospheric nitrous acid in the urban area of Beijing (China). Sci. Total Environ. 447, 210–224.
Spataro, F., Ianniello, A., Salvatori, R., Nardino, M., Esposito, G., Montagnoli, M., 2017. Sources of atmospheric nitrous acid (HONO) in the European High Arctic. Rendiconti Lincei-Scienze Fisiche E Naturali 28, 25–33.
Su, H., Cheng, Y.F., Cheng, P., Zhang, Y.H., Dong, S., Zeng, L.M., Wang, X., Slanina, J., Shao, M., Wiedensohler, A., 2008a. Observation of nighttime nitrous acid (HONO) formation at a non-urban site during PRIDE-PRD2004 in China. Atmos. Environ. 42, 6219–6232.
Su, H., Cheng, Y.F., Shao, M., Gao, D.F., Yu, Z.Y., Zeng, L.M., Slanina, J., Zhang, Y.H., Wiedensohler, A., 2008b. Nitrous acid (HONO) and its daytime sources at a rural site during the 2004 PRIDE-PRD experiment in China. J. Geophys. Res.-Atmos. 113.
Tan, Z., Rohrer, F., Lu, K., Ma, X., Bohn, B., Broch, S., Dong, H., Fuchs, H., Gkatzelis, G.I., Hofzumahaus, A., Holland, F., Li, X., Liu, Y., Liu, Y., Novelli, A., Shao, M., Wang, H., Wu, Y., Zeng, L., Hu, M., Kiendler-Scharr, A., Wahner, A., Zhang, Y., 2018. Wintertime photochemistry in Beijing: observations of ROx radical concentrations in the North China Plain during the BEST-ONE campaign. Atmos. Chem. Phys. 18, 12391–12411.
Tan, F.Z., Wang, W.J., Qi, S.F., Kan, H.D., Yu, X.P., Liu, Y., Wu, D.Y., Xu, B., Meng, F., Liu, S.E., 2019. Air pollutants and outpatient visits for cardiovascular disease in a severe haze-fog city: Shijiazhuang, China. BMC Public Health 19, 10.
Tang, Y., An, J., Wang, F., Li, Y., Qu, Y., Chen, Y., Lin, J., 2015. Impacts of an unknown daytime HONO source on the mixing ratio and budget of HONO, and hydroxyl, hydroperoxyl, and organic peroxy radicals, in the coastal regions of China. Atmos. Chem. Phys. 15, 9381–9398.
Tong, S., Hou, S., Zhang, Y., Chu, B., Liu, Y., He, H., Zhao, P., Ge, M., 2015. Comparisons of measured nitrous acid (HONO) concentrations in a pollution period at urban and suburban Beijing, in autumn of 2014. Sci. China Chem. 58, 1393–1402.
Trinh, H.T., Imanishi, K., Morikawa, T., Hagino, H., Takenaka, N., 2017. Gaseous nitrous acid (HONO) and nitrogen oxides (NOx) emission from gasoline and diesel vehicles under real-world driving test cycles. J. Air Waste Manage. Assoc. 67, 412–420.
Underwood, G.M., Miller, T.M., Grassian, V.H., 1999. Transmission FT-IR and Knudsen cell study of the heterogeneous reactivity of gaseous nitrogen dioxide on mineral oxide particles. J. Phys. Chem. A 103, 6184–6190.
Underwood, G.M., Song, C.H., Phadnis, M., Carmichael, G.R., Grassian, V.H., 2001. Heterogeneous reactions of NO_2 and HNO_3 on oxides and mineral dust: a combined laboratory and modeling study. J. Geophy. Res.- Atmos. 106, 18055–18066.
Volkamer, R., Sheehy, P., Molina, L.T., Molina, M.J., 2010. Oxidative capacity of the Mexico City atmosphere – part 1: a radical source perspective. Atmos. Chem. Phys. 10, 6969–6991.
Wang, S., Zhou, R., Zhao, H., Wang, Z., Chen, L., Zhou, B., 2013. Long-term observation of atmospheric nitrous acid (HONO) and its implication to local NO_2 levels in Shanghai, China. Atmos. Environ. 77, 718–724.
Wang, G., Zhang, R., Gomez, M.E., Yang, L., Zamora, M.L., Hu, M., Lin, Y., Peng, J., Guoc, S., Meng, J., Li, J., Cheng, C., Hu, T., Ren, Y., Wang, Y., Gao, J., Cao, J., An, Z., Zhou, W., Li, G., Wang, J., Tian, P., Marrero-Ortiz, W., Secrest, J., Du, Z., Zheng, J., Shang, D., Zeng, L., Shao, M., Wang, W., Huang, Y., Wang, Y., Zhu, Y., Li, Y., Hu, J., Pan, B., Cai, L., Cheng, Y., Ji, Y., Zhang, F., Rosenfeld, D., Liss, P.S., Duce, R.A., Kolb, C.E., Molina, M.J., 2016. Persistent sulfate formation from London Fog to Chinese haze. Proc. Natl. Acad. Sci. U. S. A. 113, 13630–13635.
Wang, J., Zhang, X., Guo, J., Wang, Z., Zhang, M., 2017. Observation of nitrous acid (HONO) in Beijing, China: seasonal variation, nocturnal formation and daytime budget. Sci. Total Environ. 587, 350–359.
Wu, L., Sun, J., Zhang, X., Zhang, Y., Wang, Y., Zhong, J., Yang, Y., 2019. Aqueous-phase reactions occurred in the $PM_{2.5}$ cumulative explosive growth during the heavy pollution episode (HPE) in 2016 Beijing wintertime. Tellus Series B-Chem. Phys. Meteorol. 71, 1620079.
Xie, Y.Z., Liu, Z.R., Wen, T.X., Huang, X.J., Liu, J.Y., Tang, G.Q., Yang, Y., Li, X.R., Shen, R.R., Hu, B., Wang, Y.S., 2019. Characteristics of chemical composition and seasonal variations of $PM_{2.5}$ in Shijiazhuang, China: impact of primary emissions and secondary formation. Sci. Total Environ. 677, 215–229.
Xing, L., Wu, J., Elser, M., Tong, S., Liu, S., Li, X., Liu, L., Cao, J., Zhou, J., El-Haddad, I., Huang, R., Ge, M., Tie, X., Prévôt, A.S.H., Li, G., 2019. Wintertime secondary organic aerosol formation in Beijing–Tianjin–Hebei (BTH): contributions of HONO sources and heterogeneous reactions. Atmos. Chem. Phys. 19, 2343–2359.
Xu, Z., Wang, T., Wu, J., Xue, L., Chan, J., Zha, Q., Zhou, S., Louie, P.K.K., Luk, C.W.Y., 2015. Nitrous acid (HONO) in a polluted subtropical atmosphere: seasonal variability, direct vehicle emissions and heterogeneous production at ground surface. Atmos. Environ. 106, 100–109.
Yang, Q., Su, H., Li, X., Cheng, Y., Lu, K., Cheng, P., Gu, J., Guo, S., Hu, M., Zeng, L., Zhu, T., Zhang, Y., 2014. Daytime HONO formation in the suburban area of the megacity Beijing, China. Sci China-Chem 57, 1032–1042.
Yu, Y., Galle, B., Panday, A., Hodson, E., Prinn, R., Wang, S., 2009. Observations of high rates of NO_2-HONO conversion in the nocturnal atmospheric boundary layer in Kathmandu, Nepal. Atmos. Chem. Phys. 9, 6401–6415.
Zhang, Q., Zheng, Y., Tong, D., Shao, M., Wang, S., Zhang, Y., Xu, X., Wang, J., He, H., Liu, W., Ding, Y., Lei, Y., Li, J., Wang, Z., Zhang, X., Wang, Y., Cheng, J., Liu, Y., Shi, Q., Yan, L., Geng, G., Hong, C., Li, M., Liu, F., Zheng, B., Cao, J., Ding, A., Gao, J., Fu, Q., Huo, J., Liu,

B., Liu, Z., Yang, F., He, K., Hao, J., 2019. Drivers of improved $PM_{2.5}$ air quality in China from 2013 to 2017. Proc. Natl. Acad. Sci. U. S. A. 116, 24463–24469.

Zhang, N., Zhou, X., Bertman, S., Tang, D., Alaghmand, M., Shepson, P.B., Carroll, M.A., 2012a. Measurements of ambient HONO concentrations and vertical HONO flux above a northern Michigan forest canopy. Atmos. Chem. Phys. 12, 8285–8296.

Zhang, Z., Shang, J., Zhu, T., Li, H., Zhao, D., Liu, Y., Ye, C., 2012b. Heterogeneous reaction of NO2 on the surface of montmorillonite particles. J. Environ. Sci. 24, 1753–1758.

Zhang, J., An, J., Qu, Y., Liu, X., Chen, Y., 2019a. Impacts of potential HONO sources on the concentrations of oxidants and secondary organic aerosols in the Beijing-Tianjin-Hebei region of China. Sci. Total Environ. 647, 836–852.

Zhang, J., Chen, J., Xue, C., Chen, H., Zhang, Q., Liu, X., Mu, Y., Guo, Y., Wang, D., Chen, Y., Li, J., Qu, Y., An, J., 2019b. Impacts of six potential HONO sources on HOx budgets and SOA formation during a wintertime heavy haze period in the North China Plain. Sci. Total Environ. 681, 110–123.

Zhang, J.W., Chen, J.M., Xue, C.Y., Chen, H., Zhang, Q., Liu, X.G., Mu, Y.J., Guo, Y.T., Wang, D.Y., Chen, Y., Li, J.L., Qu, Y., An, J.L., 2019c. Impacts of six potential HONO sources on HOx budgets and SOA formation during a wintertime heavy haze period in the North China Plain. Sci. Total Environ. 681, 110–123.

Zhang, W., Tong, S., Ge, M., An, J., Shi, Z., Hou, S., Xia, K., Qu, Y., Zhang, H., Chu, B., Sun, Y., He, H., 2019e. Variations and sources of nitrous acid (HONO) during a severe pollution episode in Beijing in winter 2016. Sci. Total Environ. 648, 253–262.

Zhang, W.H., Liu, B.S., Zhang, Y.F., Li, Y.F., Sun, X.Y., Gu, Y., Dai, C.L., Li, N., Song, C.B., Dai, Q.L., Han, Y., Feng, Y.C., 2020. A refined source apportionment study of atmospheric $PM_{2.5}$ during winter heating period in Shijiazhuang, China, using a receptor model coupled with a source-oriented model. Atmos. Environ. 222.

Zhou, X.L., Beine, H.J., Honrath, R.E., Fuentes, J.D., Simpson, W., Shepson, P.B., Bottenheim, J.W., 2001. Snowpack photochemical production of HONO: a major source of OH in the Arctic boundary layer in springtime. Geophys. Res. Lett. 28, 4087–4090.